

A synoptic climatology of potential seiche-inducing winds in a large intermontane lake: Quesnel Lake, British Columbia, Canada

Hadleigh D. Thompson^{1,2}  | Stephen J. Déry³ | Peter L. Jackson³ | Bernard E. Laval⁴

¹Natural Resources and Environmental Studies Program, University of Northern British Columbia, Prince George, British Columbia, Canada

²Centre ESCER, Department of Earth and Atmospheric Sciences, Université du Québec à Montréal, Montréal, Quebec, Canada

³Environmental Science and Engineering Program, University of Northern British Columbia, Prince George, British Columbia, Canada

⁴Department of Civil Engineering, The University of British Columbia, Vancouver, British Columbia, Canada

Correspondence

Hadleigh D. Thompson, Natural Resources and Environmental Studies Program, University of Northern British Columbia, 3333 University Way, Prince George, BC, V2N 4Z9, Canada.
Email: thompson.hadleigh@uqam.ca

Funding information

Environment and Climate Change Canada; Natural Sciences and Engineering Research Council of Canada; University of Northern British Columbia

Abstract

Excitation of basin-scale, internal waves (i.e., internal seiches) in lakes require spatially homogeneous wind fields that vary on time scales comparable to the seiche period, which can be on the order of several days in large lakes. We evaluate 2 years (October 1, 2016 to September 30, 2018) of 15-min wind data from a shore-based meteorological station to identify strong wind episodes likely to excite internal seiches in a large and geometrically complex lake surrounded by convoluted topography, Quesnel Lake, British Columbia, Canada. Our findings include the identification of strong wind event seasonality, with peak mean monthly wind speeds in April and November, and minimum mean monthly wind speeds in August. Using geopotential heights (GPHs) from $1.5^\circ \times 1.5^\circ$ gridded reanalysis data to reconstruct the atmospheric state for each strong wind episode, two primary synoptic patterns are identified that, in conjunction with local topographic channelling, lead to either easterlies or westerlies occurring at our sampling station, with strong easterly episodes three times more frequent than westerly episodes. This highlights the important role that developing low-pressure systems in the Northeastern Pacific Basin have in setting up the GPH gradient required for persistent strong winds at Quesnel Lake, in the hours and days before these storms make landfall. The projection of synoptic patterns of strong wind events onto a 4×3 self-organizing map clustered strong wind events by mean wind direction, similar to the results of a manual classification. Methods to identify the strong wind episodes and the resulting self-organizing map are both evaluated in-part by two case studies where strong winds are known to have excited a basin-scale baroclinic response in Quesnel Lake.

KEYWORDS

climatology, Quesnel Lake, seiche, self-organizing map, synoptic, wind

1 | INTRODUCTION

The interaction of the atmospheric boundary layer (ABL) with the surface of a lake provides the opportunity for

the downwards flux of momentum from the ABL to the surface and subsurface layers of the water (Spigel and Imberger, 1980; Hodges *et al.*, 2000). This transfer of momentum (henceforth *wind forcing*) can influence

many processes within a lake and is of interest to physical limnologists modelling lake hydrodynamics. In particular, wind forcing is one mechanism of exciting basin-scale waves known as seiches, which are standing waves at the surface (surface seiche) and density interfaces (internal seiche; Antenucci and Imberger, 2003; Gardner *et al.*, 2006).

Internal seiches in Quesnel Lake, British Columbia (BC), have been previously cited for their role in the lake's downstream temperature fluctuations (Laval *et al.*, 2008), and potential sediment re-suspension (Petticrew *et al.*, 2015). A mine tailings spill into Quesnel Lake on August 4, 2014 provides motivation for further physical limnology research, including the need to clarify the role of wind forcing in seiche events in this morphometrically complex basin. This research is part of a larger inter-disciplinary investigation to understand the long-term physical, chemical, and biological effects of the spill (see Petticrew *et al.*, 2015; Hatam *et al.*, 2019).

The mechanism that initiates a wind-forced seiche response in a lake is the piling of lake water towards the downwind end of the basin by the drag exerted by persistent, spatially homogeneous winds (Laval *et al.*, 2003; Valerio *et al.*, 2017), which results in a tilted lake surface, known as setup. At steady state, there will be a balance in the water column between surface drag and the ensuing barotropic pressure gradient (Heaps, 1984). If the lake is thermally stratified (a two-layer density stratification approximation is sufficient), the thermocline adjusts to the baroclinic pressure gradient by tilting in the opposite direction until, at steady state, the baroclinic and barotropic pressure gradients balance. Rapid changes in wind forcing will allow an oscillatory response of the thermocline similar to a forced, damped oscillator, which is known as a baroclinic, or internal, seiche (see Spigel and Imberger, 1980; Imam *et al.*, 2013). The wind duration required for the thermocline to first reach equilibrium tilt is one quarter of the fundamental seiche period of the basin (i.e., $T/4$; Stevens and Lawrence, 1997). During summer stratification, Quesnel Lake has a seiche period of about 6 days, thus wind events must be at least ~ 1.5 days long to excite a baroclinic seiche response (Laval *et al.*, 2008).

To date, few studies have encapsulated the role of synoptic-scale forcing on seiche activity, notable exceptions being the identification of 'meteorological tsunamis', where a phenomenon similar to an enclosed water-body's internal seiche is seen in coastal inlets. Meteorological tsunamis are forced by low-frequency, high-amplitude disturbances of atmospheric pressure (Rabinovich and Monserrat, 1998; Marcos *et al.*, 2009). Comparable research to this present study includes seiche activity observed in Rotterdam Harbour, where wind data from a shore-based meteorological station were

related to the passage of cold fronts and their associated post frontal convection cells (de Jong and Battjes, 2004). However, research of the large-scale atmospheric patterns that influence hydrodynamics in intermontane or sub-alpine lakes is currently missing from the literature.

In this article, we present an environment-to-circulation synoptic climatology (see Yarnal, 1993; Yarnal *et al.*, 2001) focused on a limited number of strong wind events that meet the criteria to initiate baroclinic seiching. Our main goals are to quantify the frequency and duration of these strong wind events, improve understanding of the synoptic conditions required to force such events, and to visualize the synoptic-scale atmospheric patterns responsible with the use of a self-organizing map (SOM).

2 | DATA AND METHODS

2.1 | Study area

Quesnel Lake, BC's deepest inland body of water, is nestled into the western slopes of the Cariboo Mountains, and is a glacial-scoured, fjord-type, oligotrophic lake (Laval *et al.*, 2012). The three arms of Quesnel Lake span $121^{\circ}34'22''\text{W}$ to $120^{\circ}20'45''\text{W}$ in longitude (~ 83 km), and $52^{\circ}27'46''\text{N}$ to $52^{\circ}46'51''\text{N}$ in latitude (~ 35 km). The Main Basin is a deep (~ 500 m), central area of the lake that encompasses the intersection of the three arms that protrude east, north, and west, respectively. The West Basin is a portion of the western arm of the lake that is oriented northwest to southeast and is separated from the Main Basin by a shallow (~ 30 m) sill (Figure 1). The lake's mean width of 2.7 km coupled with the eastern portions being flanked by the Cariboo Mountains results in the lake being mostly surrounded by complex mountainous topography, which has the potential to cause local wind flow phenomena seen in similar terrain by Valerio *et al.* (2017), such as channelling of flow, lee-side separation, and valley breeze circulations.

The climate of the Cariboo Mountains has been categorized as transitional by Beedle *et al.* (2015), as they are drier than the Coast Mountains to the west, yet wetter than the Rocky Mountains to the east (Sharma and Déry, 2016). Elevations range from 330 m above sea level (masl) to 3,520 masl. Throughout the text, we utilize the boundaries and terminology of the 7,700 km² Cariboo Mountains Region, as identified by Sharma and Déry (2016).

2.2 | Near-surface meteorological data

Data used for identifying strong wind episodes were obtained from an automated meteorological station at

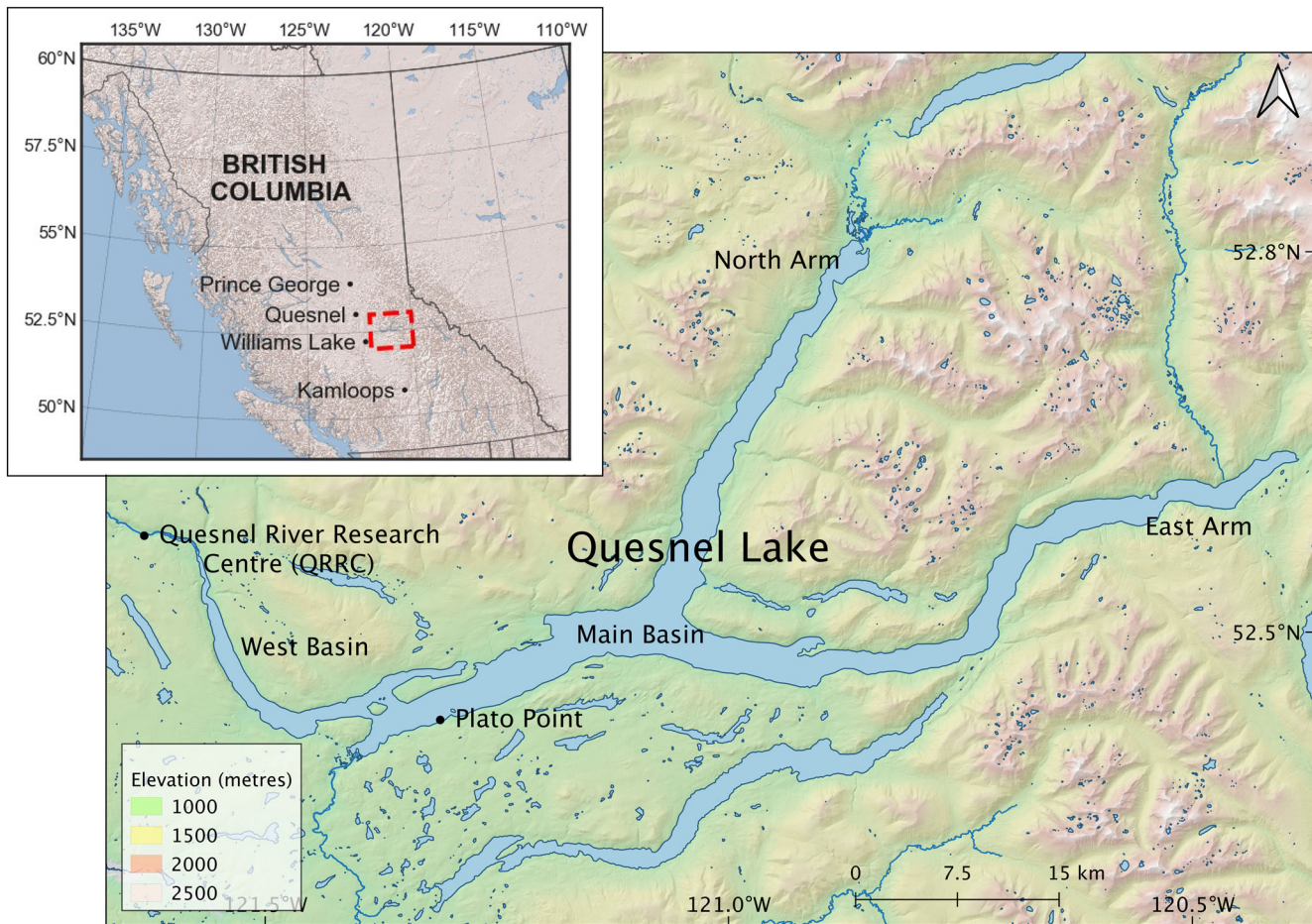


FIGURE 1 Quesnel Lake and the location of the Quesnel River Research Centre and Plato Point. Inset: The location of Quesnel Lake within British Columbia (red square), and the locations of four ECCC stations providing long-term wind data. ECCC, Environment and Climate Change Canada [Colour figure can be viewed at wileyonlinelibrary.com]

Plato Point (Hernández-Henríquez *et al.*, 2018), which is located on the southern shore of Quesnel Lake's Main Basin (52°29'14"N, 121°17'03"W, 728 masl) (Figure 1), and has been in operation since August 2016. The site is exposed to open water from ~230°, through North, to ~110°, with Plato Island lying ~250 m offshore covering an arc of ~2° to ~55°. The station sits on a gently sloping gravel shoreline ~25 m wide (depending on lake height), and the area south of the site is dominated by a mature coniferous forest. We use the Plato Point station as it provides the longest record of 15-min interval lake-level wind observations within the catchment. The station records average wind speed, wind speed *SD*, average wind direction, and instantaneous wind direction for each 15-min interval. The station uses a RM-Young four-vane propeller wind monitor with accuracies of $\pm 0.3 \text{ m s}^{-1}$ and $\pm 3^\circ$ for wind speed and wind direction, respectively. The cross arm supporting the anemometer is mounted 2.7 m above the surface. Quality control was performed on the dataset by ensuring all values were

within ranges that made physical sense (i.e., 0–360° for wind direction, wind speeds $\geq 0.0 \text{ m s}^{-1}$), however, no observations were required to be excluded. We use 15-min wind data from Plato Point station with the assumption that they represent wind conditions throughout the Main Basin, and over a longer time scale (e.g., daily averages) can be representative of wind conditions over the entire lake.

While the two-year study period (see Section 2.3) is relatively short for a climatological analysis, collecting long-term, high-frequency (sub-hourly) data in a remote location such as Quesnel Lake comes with many technical and logistical challenges (see Hernández-Henríquez *et al.*, 2018). As such, we have therefore maximized the currently available data over a period of study that coincides with an intensive effort to collect limnological measurements following the Mt. Polley incident (Petticrew *et al.*, 2015).

The climatology of wind over the Cariboo Mountain Region derives from 25 years (January 1981–December

2005) of (near-)continuous hourly data from four Environment and Climate Change Canada (ECCC) stations bordering the region (Figure 1 inset). Monthly mean wind speeds display a seasonal signal with peaks in both April and November, and the lowest mean monthly wind speeds occurring in August (Figure 2). We therefore delineate January to May, and October to December, as two separate active seasons centred around the local maxima in wind speeds, and June to September as a calm season. These three seasons are then used to evaluate if strong wind events and the associated synoptic patterns display a seasonal signal, and to assist in identifying the start and end points for the near-surface wind data time series.

2.3 | Identifying and quantifying strong wind events

A two-year time series from October 1, 2016 to September 30, 2018 from Plato Point is chosen for consistency with the three identified wind seasons. There were no missing values from the raw 15-min dataset covering this period, resulting in 70,080 observations. Standardized mean monthly wind speed values from this time series display good agreement with data from the four ECCC stations during October 1, 2016 to September 30, 2018 (Figure 2). Spearman rank correlation-coefficient values between normalized wind speeds at Plato Point and the four ECCC stations ranged from 0.79 to 0.96 (all with $p < .05$), with an average correlation coefficient of 0.90 ($p < .05$). These results provided confidence in the use of the 25-year dataset to estimate wind seasonality at Quesnel Lake. The 15-min wind speed observations in the raw wind speed dataset were squared and then averaged over each hour to derive a time series of mean hourly values that were proportional to the wind stress at the lake

surface, with units of $\text{m}^2 \text{s}^{-2}$. This was smoothed by a 36-hr moving average, similar to Laval *et al.* (2008), which represents one quarter of the fundamental seiche period for the main east–west thalweg portion of the lake during summer stratification. The smoothed hourly time series will from hereon be denoted as U^2 . Wind stress or U^2 values are preferred over raw wind speeds as they highlight periods of greater forcing for wind-momentum driven hydrodynamic processes.

The methods developed here for delineating strong wind episodes at Quesnel Lake are motivated by similar work examining mid-latitude storm occurrence in Perth, Australia by Breckling (1989). For an episode to be recorded, wind stress values must have exceeded the 80th percentile of the mean annual U^2 value ($12.5 \text{ m}^2 \text{ s}^{-2}$) for a continuous period of ≥ 36 hr. The 80th percentile was chosen after trials with various thresholds. The aim was to identify a value low enough to allow a sufficient number of episodes to be identified, while high enough for episodes to have an effect on lake hydrodynamics. The minimum episode duration of 36 hr originates from the required setup duration in this lake. Parameters derived from the U^2 time series for each episode are provided in Table 1 with a graphical example of the procedure in the Supporting Information (Figure S1).

A total U^2 for an episode was calculated by summing the hourly U^2 values over the duration of the episode and used as a measure to assist in statistically comparing the various episodes within this study. Wind steadiness (S ; the mean hourly wind vector divided by the mean hourly wind speed) was included to provide a measure of the constancy of the direction during each event (Singer, 1967). A complete table of the episodes is provided in the Supporting Information (Table S1).

The filtered episodes were then categorized using two main criteria: (a) by the three wind seasons identified in Section 2.2 and (b) by the mean wind direction during

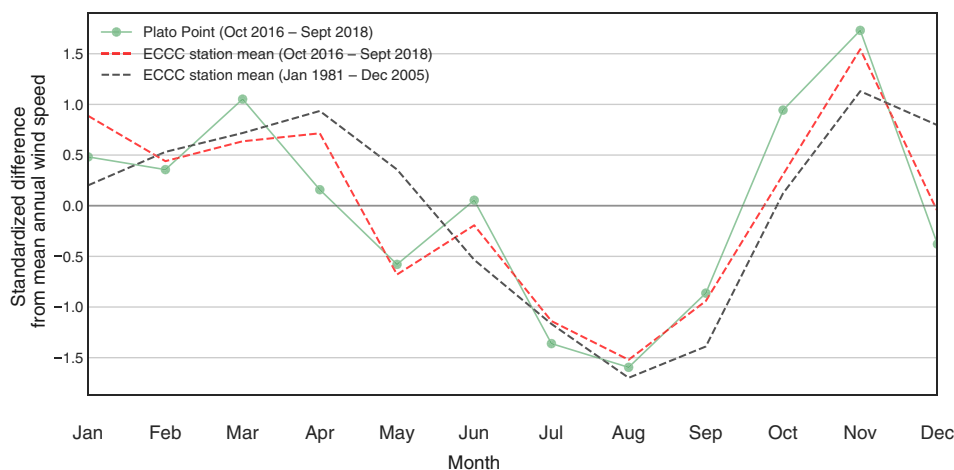


FIGURE 2 Standardized mean monthly wind speeds at Plato Point, Quesnel Lake, for the period October 1, 2016–September 30, 2018. The mean of four ECCC stations bordering the Cariboo Mountain region for the same period is in red, while the climatological mean (1981–2005) of the four ECCC stations is indicated in black. ECCC, Environment and Climate Change Canada [Colour figure can be viewed at wileyonlinelibrary.com]

TABLE 1 Values derived from the strong wind episode filtering procedure outlined in Section 2.3

	Parameter	Units
1.	Start date/time	Pacific daylight time
2.	End date/time	Pacific daylight time
3.	Duration	Hours
4.	Date/time of maximum U^2	Pacific daylight time
5.	Mean wind direction	Degrees
6.	Wind direction SD	Degrees
7.	Wind steadiness	-
8.	Mean U^2	$m^2 s^{-2}$
9.	Total U^2	$m^2 s^{-2}$

each episode. This was to investigate if differences exist in the frequency of episodes based on these two categories. The occurrence of episodes per month is also provided. We use Welch's t test for assessing the significance of differences, choosing a p -value threshold of .05 (Delacre *et al.*, 2017).

2.4 | ERA-interim reanalysis data

To determine the large-scale atmospheric forcing for each strong wind event, synoptic data of geopotential height (GPH) at 925, 800, and 500 hPa were downloaded from the European Centre for Medium Range Weather Forecasts' (ECMWF's) ERA-Interim reanalysis archive (<http://www.ecmwf.int/research/era>). The selected heights of 925, 800, and 500 hPa correspond to lake level, the surrounding ridgetops, and the above ridgetop free atmosphere, respectively. The ERA-Interim product spans January 1979–August 2019, has a spatial resolution of 1.25° , and is available on 60 vertical pressure and model levels (Berrisford *et al.*, 2009; Dee *et al.*, 2011). Data are available at the synoptic hours of 0000, 0600, 1200, and 1800 UTC. We denote the time of maximum U^2 for each episode as T-0, obtaining data as close as possible to T-0 and for the synoptic hours 24 and 48 hr prior (T-24 and T-48, respectively). If T-0 fell in between synoptic hours (e.g., 0900 UTC), the time was rounded forward to the next synoptic hour, thus capturing as much of the event as possible.

Data were initially downloaded covering a domain of 35° – 65° N, and 100° – 180° W, at resolutions of $1.5^\circ \times 1.5^\circ$ (1,200 grid points) and at $2.5^\circ \times 2.5^\circ$ (432 grid points). This is a larger domain than used in similar studies by Bakri *et al.* (2017) and Stahl *et al.* (2006); however, the long duration of several strong wind episodes meant that a larger 'upstream' view would allow adequate visualization of the synoptic patterns in the Northeastern Pacific Basin.

A manual clustering of GPH patterns into similar groups at three time steps (T-0, T-24, and T-48) for each event was performed to verify if recurring patterns were identifiable to a human observer, and to provide an understanding of the variety in atmospheric states. The procedure was analogous to the manual methods recommended for early career practitioners by Yarnal (1993), whereby maps of similar composition were clustered together depending on their synoptic features such as the locations of low-pressure systems, short-wave troughs, and high-pressure ridges.

2.5 | The self-organizing map

The SOM, first presented by Kohonen (1982), is a form of unsupervised machine learning that acts as an automated method to cluster similar GPH patterns together. The general principle behind a SOM is that input vectors are clustered at nodes on a two-dimensional grid where the Euclidean distance is the lowest for data that are similar, and further apart for data that are dissimilar (Kohonen *et al.*, 2001; Kohonen, 2003; Sheridan and Lee, 2011). An advantage a SOM has over other clustering methods is its ability to reduce the complexity of multi-dimensional data, allowing the input vector to contain information about multiple variables (e.g., pressure, temperature, precipitation); this inclusion of various parameters can allow for a more detailed description of the state of the atmosphere (Skific and Francis, 2018).

Many climatology studies use SOMs as a diagnostic tool when processing large datasets, which would otherwise have been impossible to cluster using manual methods, or in situations where the results provide a clearer picture of the atmospheric states than by using other computer-assisted methods (e.g., empirical orthogonal functions, compositing, k-means clustering; Grotjahn *et al.*, 2016). However, we propose the use of a SOM in this study as a tool for projecting the continuum of synoptic states that are present during the strong wind events at Quesnel Lake, which is a novel use for SOMs in a low observation, environment-to-climate synoptic climatology. This method allows for a greater variety of synoptic states to be viewed at once than by using manual methods, compositing, or k-means clustering.

In this study, an input vector (also known as an observation) is a single-dimensional representation of gridded GPH anomalies at a specified time. The first step taken to create an observation was to reshape an $M \times N$ grid of ERA-Interim data to a one-dimensional vector of length $M \times N$. These were standardized over the spatial domain to derive GPH anomalies, which removes the magnitude and reduces the disproportionate influence of a single

variable or outlier (Schuenemann and Cassano, 2010). Each vector point was then area-weighted by multiplying it by the square root of the cosine of the latitude that it originated from. This area-weighting is required because a standard latitude/longitude grid is not uniform in shape, which results in grid points near the equator accounting for greater area than grid points near the poles (Loikith *et al.*, 2017). Standardized, area weighted vectors from the 925 and 500 hPa levels at each T-0 timestep were concatenated together to form an input vector that was of length $M \times N \times 2$. These represent the synoptic state at the peak of each strong wind event. The final form of each input vector made up of $M \times N \times 2$ grid points is given by:

$$\text{vector}_i = [X_1^{925}, X_2^{925}, X_3^{925} \dots X_{M \times N}^{925}, X_1^{500}, X_2^{500}, X_3^{500} \dots X_{M \times N}^{500}] \quad (1)$$

SOM input vectors derived from the larger domain (see Section 2.4) produced inconclusive results, and a secondary, smaller domain covering 47.0° – 57.5° N, and 112.5° – 130° W at a resolution of $1.5^\circ \times 1.5^\circ$ (117 grid points) improved the SOM performance. This change reduced the computational requirements of the SOM procedure and also located Quesnel Lake at the centre of the domain, in line with recommendations by Gibson *et al.* (2017).

The SOM algorithm was implemented using the Python miniSOM library (Vettigli, 2019). The final method and successful values used for the learning rate, neighbourhood distance decay, and number of iterations (all outlined by Hewitson and Crane, 2002), are discussed in Section 3.2.

2.6 | Comparison with known periods of interest

We investigate two episodes where a hydrodynamic response to wind forcing within Quesnel Lake has been observed and use the associated data to compare the methods developed herein to identify strong wind episodes and to evaluate the manual analysis and SOM results.

The first case relies on previous research by Laval *et al.* (2008), where westerly wind events generated baroclinic seiches in the West Basin during August 2003. The date and timing of the strongest period of wind are taken directly from the literature and are based on in-situ measurements. Applying the nomenclature used thus far, T-0 (the hour of maximum wind forcing) occurs at 0000 UTC August 3, 2003. The second case is highlighted due to particularly high bottom-layer horizontal velocities

observed in the West Basin by a limnology research group (B. Granger, personal communication, September 29, 2018). Easterly winds moved surface water towards the outlet of the Quesnel River, creating a return current at the bottom of the basin. Peak bottom-layer velocities were observed at 0800 UTC November 26, 2016 and the closest synoptic hour of 0600 UTC November 26, 2016 is used as T-0. An event at this time is identified by the data filtering method from Section 2.3 and is listed in Table S1 as episode # 10. Synoptic data are obtained for these two events as discussed in Section 2.4 and transformed into new input vectors for the master SOM. The resulting node location compared with the trained master SOM is used to evaluate the SOM method.

3 | RESULTS

3.1 | Strong wind episodes

During the 24-month period from October 1, 2016 to September 30, 2018, 47 strong wind episodes were identified using the methods outlined in Section 2.3. The monthly distribution of strong wind episodes appears similar to the seasonal signal in mean monthly wind speeds over the region identified in Section 2.2; a peak in episode occurs in March, and again in November, with no strong wind episodes in August and September (Figure 3).

All events are constrained to wind directions between 90° and 270° ($90^\circ < D < 270^\circ$; Figure 4). This is partly due to the synoptic forcing and the resulting GPH gradient, but also evidence of wind channelling by the surrounding topography. The grouping of larger circles near $15 \text{ m}^2 \text{ s}^{-2}$ to $30 \text{ m}^2 \text{ s}^{-2}$ from the direction of $\sim 120^\circ$ indicates that the synoptic patterns related to the strongest episodes may not have a large amount of inter-event variability (Figure 4). No episodes having northerly winds were recorded at Plato Point. Additionally, although there are events with southerly components, it was determined during the manual synoptic map classification that there was no separate identifiable atmospheric pattern responsible for these southerly winds. Therefore, two classes of synoptic patterns are present and the resulting strong wind episodes can be delineated into easterlies (mean wind direction from 0° to 179°) or westerlies (mean wind direction from 180° to 359°).

There are 37 easterly events accounting for the majority of cases (79%) throughout the 2 years. November experiences the most easterly episodes, while 10 westerly events (21%) are distributed over the months of February to October, with a peak occurrence

FIGURE 3 Monthly occurrences of strong wind events at Plato Point over the period October 1, 2016–September 30, 2018, stratified by wind direction. Easterlies lie between 0° and 179° , westerlies between 180° and 359° . The number of episodes has been standardized by the number of total occurrences [Colour figure can be viewed at wileyonlinelibrary.com]

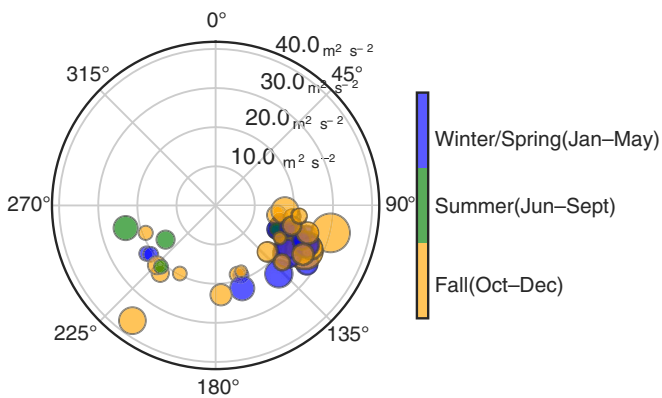
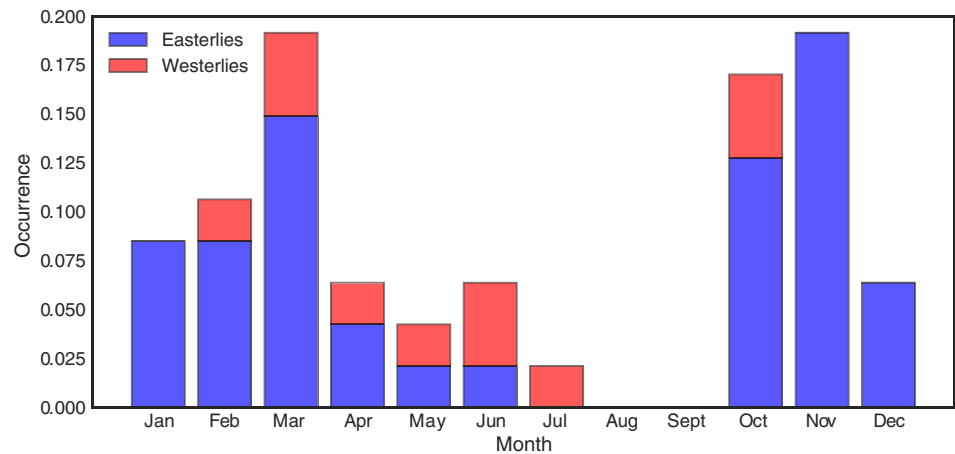


FIGURE 4 Windrose of 47 strong wind events recorded during October 1, 2016–September 30, 2018. Directions follow standard meteorological convention. The radial axis of the windrose represents the mean wind stress during the episode. The size of each bubble represents the total wind stress during the episode, but sizes have been altered to allow for easier comparisons: The smallest bubble represents $613 \text{ m}^2 \text{ s}^{-2}$ while the largest represents $2,204 \text{ m}^2 \text{ s}^{-2}$. Intermediate values follow a linear scale [Colour figure can be viewed at wileyonlinelibrary.com]

in June. Easterly events have a median duration of 49 hr compared to westerly events that last 41 hr; however, this difference was not statistically significant (Welch's t test: $\text{stat} = -1.755$, $p = .095$; Table 2). Easterly events also have total U^2 values of $1,028 \text{ m}^2 \text{ s}^{-2}$ compared to the westerlies value of $918 \text{ m}^2 \text{ s}^{-2}$; again, this difference was not statistically significant (Welch's t test: $\text{stat} = -1.04$, $p = .309$). No statistical tests were applied to the differences between wind seasons due to the large sample size differences. Events during the calmer summer season have similar durations as events during the more active months yet have a lower average wind stress and therefore lower total U^2 values. The mean wind direction during the summer is 218° , compared to 125° and 135° during fall and winter/spring, respectively.

3.2 | The projection of synoptic patterns using a self-organizing map

From the manual analysis, we determined that a human observer would cluster the maps of the 47 events into two distinct groups, dependent on the mean wind direction (i.e., westerly or easterly). The compositing of events by this grouping indicated that easterly winds are driven by an east-to-west GPH gradient over central BC established by mid-latitude cyclone development in the Gulf of Alaska and the Northeastern Pacific Basin, with the surface low-pressure system being supported by an upper-level trough lying to the west (off-shore) of coastal BC (Figure S3a). Conversely, westerly winds require a west-to-east GPH gradient that is produced when a high-pressure ridge exists off the coast of BC. The axis of a short-wave trough lying to the east of central BC also emerges, likely having recently passed through the study area (Figure S3b). However, the compositing of images from all events performs poorly in representing the variety of synoptic patterns, a task for which we utilize a SOM.

Multiple SOM trials were conducted with input vectors from the smaller domain described in Section 2.5, to test a variety of input parameters and SOM dimensions. The successful 4×3 (four rows, three columns) SOM used a learning rate of 0.35 and a distance decay value of 1.0. Applying random initial weights gave better results than using weights derived from a principal component analysis, as did using a random training method in place of the batch training method. The trained SOM will be referred to from hereon as the *master SOM*. This is common practice as many other SOM variations can be derived from the successful master SOM configuration (Schuenemann and Cassano, 2010; Sheridan and Lee, 2011). The nodes are designated by row and column locations on the map, making the top left node (1,1) and the bottom right node (4,3).

TABLE 2 Median and *SD* (in brackets) values^a for quantities calculated during strong wind episodes at Quesnel Lake during October 1, 2016 to September 30, 2018

	Occurrences	Duration (hours)	Mean wind direction (degrees)	Mean U^2 ($m^2 s^{-2}$)	Total U^2 ($m^2 s^{-2}$)
Winter/spring	23	46.0 (13.9)	135 (48)	21.4 (4.6)	1,028 (398)
Summer	4	48.0 (12.2)	218 (56)	18.8 (3.3)	917 (268)
Fall	20	48.0 (9.8)	125 (35)	21.1 (3.2)	997 (263)
Easterlies	37	49.0 (12.6)	118 (20)	20.2 (3.7)	1,028 (357)
Westerlies	10	41.0 (9.0)	229 (14)	21.8 (5.1)	918 (244)

^aMean wind direction values are given as circular mean and circular *SD*.

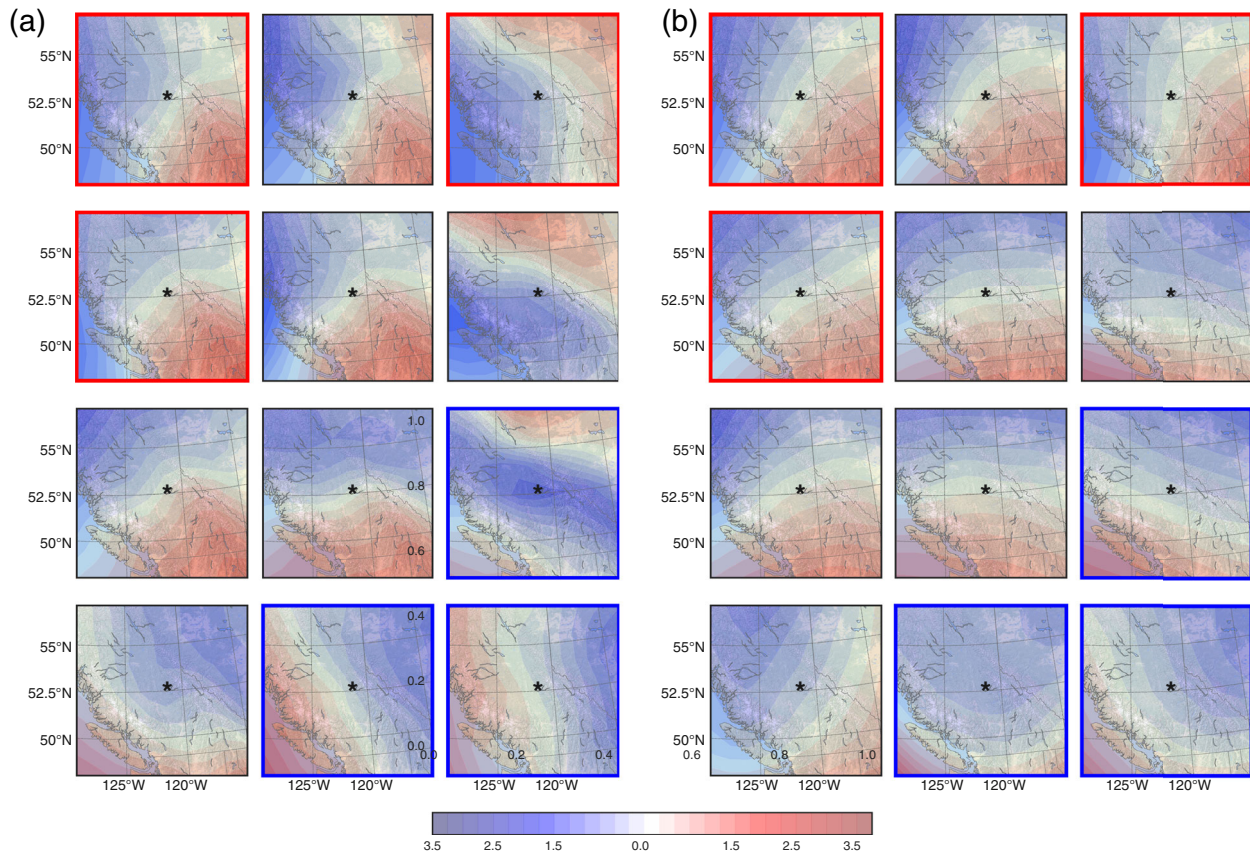


FIGURE 5 The 4×3 master SOM of (a) 925 hPa, and (b) 500 hPa GPH anomalies, derived from the output vectors described in Section 2.5. Anomaly increments (unitless) are 0.25 per shaded contour. Red boxes indicate clusters of multiple easterly wind episodes and blue boxes represent the same for westerly episodes [Colour figure can be viewed at wileyonlinelibrary.com]

The success of the master SOM was measured by the grouping of strong wind episodes by the mean wind direction during the episode (Figure S2). There is a clear distinction between easterly events, clustered primarily along the left and top of the map, and the westerly events that are clustered to the bottom right. Again, the seasonality of events is not captured by the SOM, which would have been evident by an ordered arrangement of the coloured labels across the map in Figure S2. The SOM is allowing the projection of a continuum of the possible synoptic states that drive strong

wind events at Quesnel Lake, arranging them by the alignment of the GPH gradient over the region. Where multiple events are clustered together on nodes [e.g., nodes (1,1), (1,3), (2,1), and (4,3)] the SOM has determined that the input vectors are similar. To visualize the composite of events at each node of the SOM, output vectors are derived by taking the mean of the input vectors clustered at each location and split into two. Grids of 925 and 500 hPa GPH anomalies are then reconstructed from the two output vector components (Figure 5).

To quantify the proportion of synoptic patterns explained by each output vector, the number of easterly or westerly events clustered at each node was divided by the total number of easterly or westerly events, respectively. Red (for easterlies) and blue (for westerlies) boxes are used in Figures 5 and 6 to denote the three nodes that account for the greatest number of events per classification. Nodes (1,1) (27.0%), (1,3) (18.9%), and (2,1) (13.5%), account for a total of 59.4% of the variance in easterly episodes. The rest of the easterly events are distributed across the remainder of the SOM, except at nodes (1,3) and (2,1). Output vectors at nodes (4,2) and (4,3) represent 80% of the total variance of the westerly events, with the vectors at nodes (4,1) and (3,3) representing 10% each. This analysis of the proportion of synoptic patterns can also be thought of as an indicator of the likelihood of occurrence for the pattern at each node. The approach of reducing the size of the input domain and the location of Quesnel Lake relative to the domain boundaries contributed to the improved performance of the SOM algorithm; however, to visualize the atmospheric forcing for the strong wind events synoptic patterns of GPH covering the larger domain were projected onto a 4×3 grid, utilizing the layout of the master SOM as a template.

The resulting SOMs for the two GPH levels of 925 and 500 hPa are used to interpret the large-scale forcing for strong wind episodes (Figure 6). Three main easterly nodes [(1,1), (1,3) and (2,1)] are all dominated by a surface closed low off the coast of BC at 925 hPa, with an associated shortwave trough at 500 hPa (Figure 6). The most common pattern at node (1,1) has the closed low situated high in the Gulf of Alaska, with Quesnel Lake located in between the axes of the 500 hPa trough and ridge. This pattern closely resembles the composite of easterly events in Figure S3 and is also comparable to the patterns responsible for inflow events on the BC coast identified by Bakri *et al.* (2017), which are also orientated east-to-west. Our analysis shows that this pattern is most likely during fall and winter (Figure S2), which agrees with previous literature identifying the seasonal occurrence of atmospheric patterns over western Canada (Stahl *et al.*, 2006), Ridging to the west of BC that is fundamental for the west–east GPH gradient associated with strong westerly events is evident at both levels in the three westerly nodes [(3,3), (4,2) and (4,3)]. Node (4,3), the highest occurrence of westerly events, displays the greatest ridge amplitude of the three westerly nodes at both the 925 and 500 hPa levels, with a downstream trough axis to the east of Quesnel Lake present at 500 hPa, is most similar to pattern 2 identified by Stahl *et al.* (2006) that has its highest frequency during the summer months. This indicates that the pattern at node (4,3) could be responsible for strong westerly episodes

during the months of July and August that may occur outside of our limited study period. Nodes without red or blue boxes represent outliers or patterns that defy physical interpretation. For example, node (1,2) represents a strong low-pressure system that although realistic, has a low probability of occurrence (i.e., 1 out of 47). Conversely, the averaging of both easterly and westerly events at node (4,1) results in a pattern that is unlikely in real-world atmospheric flow (Figure 6a).

3.3 | Case studies of known seiching events

The westerly event in August 2003 resulted from the combination of a weak high-pressure system in the Gulf of Alaska and a closed low northeast of northern BC, observed at 925 hPa (not shown). This is supported in the mid-troposphere by a broad ridge west of the BC coast and a shortwave trough located above the surface low. These combinations induce a west-to-east GPH gradient observed over most of BC. The weakness of the ridge and length of the associated long-wave are noticeably different to the other previously identified westerly events. The associated GPH gradient observed across the smaller domain however, is similar to the mean of patterns clustered at node (4,2) in the master SOM (Figure 7). The easterly event in November 2016 follows the pattern of an intense low-pressure system approaching the coast of BC, either originating, or having been strengthened by, the Aleutian low (Figure S4). In the 500 hPa pattern, there exists a closed low in the mid-troposphere at T-48 which weakens to a shortwave trough at T-24. Of note is the trajectory of the system, whereby the SE movement of the storm prevents it passing directly over central BC. This is important for the persistence of the strong wind episode, which otherwise would have had a shorter duration and a probable wind shift after the passage of the associated cold front. The intensity of the GPH gradient surrounding the closed low at T-48 and T-24 compared to T-0 is also interesting considering that T-0 in this instance represents the occurrence of peak hydrodynamic response observed in the lake. At T-0 the low appears to have already begun to dissipate, possibly due to orographic effects as the system made landfall, yet this time lag raises pertinent questions about how the complex basin geometry of Quesnel Lake responds to wind forcing in the hours and days after its application.

A trained master SOM can evaluate further data by assigning any new observation vectors (i.e., 925 and 500 hPa maps) to a ‘winning’ node on the map. This is achieved by the SOM computing which node has the smallest Euclidean distance from the new input vector.

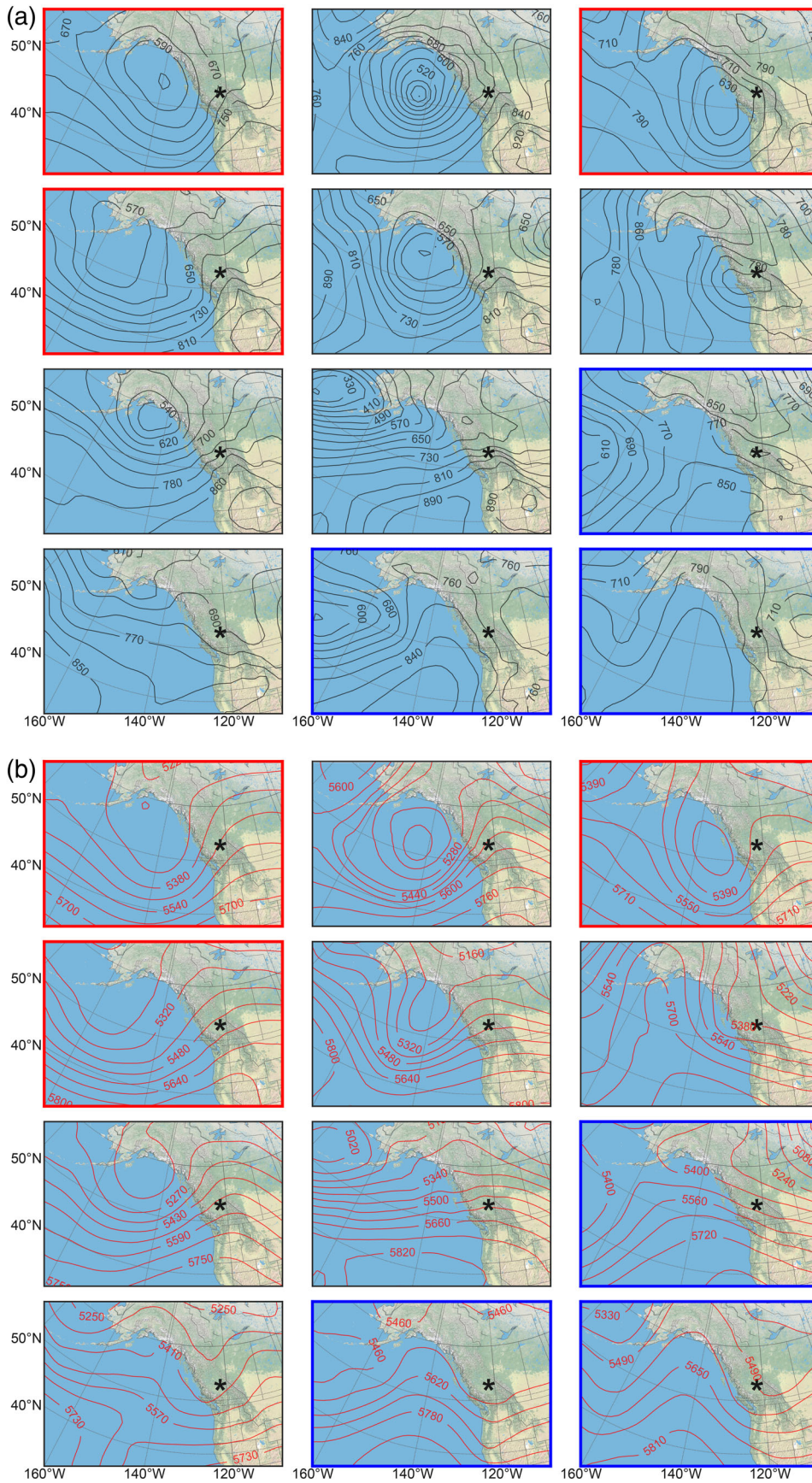


FIGURE 6 The projection of clustered (a) 925 hPa and (b) 500 hPa GPH patterns using the master SOM template, in the same format as Figure 5. All heights are in metres (m). Panels outlined in red (easterlies) and blue (westerlies) represent patterns that account the majority of the input variability, as outlined in Section 3.2. GPH, geopotential height; SOM, self-organizing map [Colour figure can be viewed at wileyonlinelibrary.com]

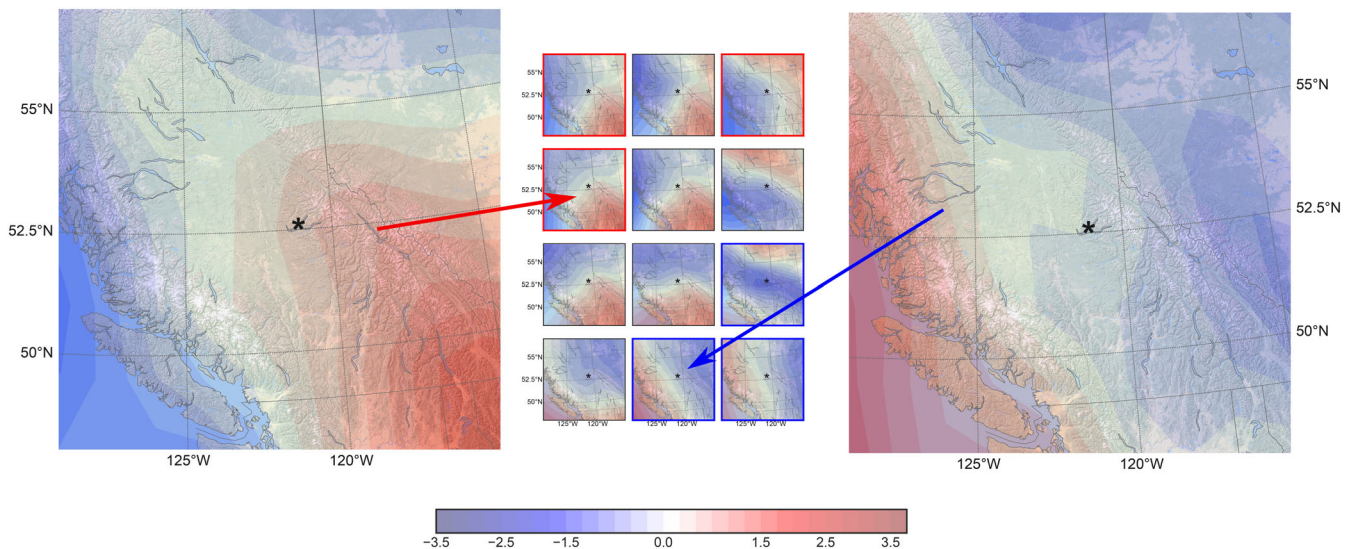


FIGURE 7 Winning nodes on the master SOM for the two case study events outlined in Section 2.6. The easterly event (left) was allocated to node (2,1); the westerly event (right) to node (4,2). The centre image originates from Figure 5. All panels are of standardized 925 hPa GPH anomalies, and shaded contours are in 0.25 (unitless) increments. GPH, geopotential height; SOM, self-organizing map [Colour figure can be viewed at wileyonlinelibrary.com]

SOM input vectors for the two cases mentioned above were constructed using the methods described in Section 2.3 (using the smaller domain). These were then evaluated by the master SOM and allocated to the appropriate nodes. This technique is not an infallible validation method, as the SOM will always allocate the new observation to a node on the map rather than reject it, complicating the analysis; however, the easterly event was allocated to node (2,1), and the westerly event to node (4,2) (Figure 7), both of which had already been identified as significant in Section 3.2.

4 | CONCLUDING DISCUSSION

By analyzing hourly wind stress data to identify episodes of strong winds at Quesnel Lake, we compiled a synoptic climatology for the large-scale atmospheric patterns that drive these events. Over a two-year period (October 1, 2016–September 30, 2018), there were 37 episodes of strong easterly winds, compared to 10 westerly events. Episodes last for an average duration of 47 hr. Easterly episodes are possible during all seasons, with peaks in the spring (March) and fall (November). Westerly events also occur throughout the year but dominate during June and July. No events were observed during August or September. The mean wind direction of all episodes falls between 90° and 270° (through 180°), highlighting the topographic effects of the surrounding Cariboo Mountains. Composites were assembled from the mean of all

episodes associated with easterly or westerly winds observed at Quesnel Lake. The easterly composite reveals the influence of developing low-pressure systems from the Gulf of Alaska have on the GPH gradient over central BC. The east-to-west setup persists as the systems track southeast, allowing wind stress on the lake to accrue. Westerly winds develop with strong ridging in the lower to mid troposphere to the west of the BC coast, which at times is assisted by the passage of a shortwave trough over central BC, exacerbating the west-to-east GPH gradient. To visualize the full array of atmospheric patterns a SOM was used to project the synoptic maps and to cluster episodes that the algorithm deemed similar. The resultant 4×3 master SOM was able to allocate every input vector to a node and therefore span the full data space of observations, an advantage the technique has over other non-hierarchical clustering methods. Two separate regions of nodes were identified as being significant for the easterly and westerly episodes, explaining 59 and 90% of the variance, respectively.

Finally, two case studies of strong wind events known to drive internal hydrodynamic processes within the lake are examined and used to validate the data filtering, manual synoptic analysis, and SOM projection methods. These case studies have allowed for an analysis of one easterly and one westerly episode. Although outside of the study period, the westerly event observed in 2003 is important due to the uniqueness of the collocated meteorological and limnological observations. This event also highlights the potential for summertime wind-forcing

despite the methods used herein not identifying any during the October 2016–September 2018 study period. The easterly event that occurred within our study period, provides justification for the data filtering methods, yet also highlights the further research required to couple the timing of peak wind stress with the lake's hydrodynamic response. For both cases, the resulting synoptic patterns show good agreement with the manual analysis and the SOM results. Both events were able to be allocated to nodes on the SOM already highlighted for their significance in the ability to explain variance within the synoptic dataset.

This climatology of high wind episodes that potentially induce seiching in Quesnel Lake contributes to a broader effort to monitor the impact of the 2014 tailings pond spill from the Mt. Polley Mine on the physical, chemical and biological processes in the lake (Petticrew *et al.*, 2015). There is mounting evidence that tailings pond sediments deposited at the bottom of the lake's West Arm become resuspended seasonally due to internal-seiche motion, with a multi-year decay in magnitude of resuspension since the spill (Hamilton *et al.*, in preparation). Furthermore, the exchange of suspended material between Quesnel Lake's West Basin (where most of the initial mine spill material was sequestered) and its Main Basin is mediated by these same internal-seiche motions. As a subsequent effort, we plan to interpret the combined atmospheric and limnological processes (i.e., wind-induced seiching) that may lead to resuspension of sediments from the lake bottom beyond the two-years of observations used in this study. Indeed, there is an ongoing effort to monitor lakeshore wind and other meteorological conditions at five sites to potentially capture high-wind events, including the rare occurrences during August and September.

ACKNOWLEDGEMENTS

The authors thank Michael Allchin and the staff of the Quesnel River Research Centre, field assistants of the Northern Hydrometeorology Group (UNBC), Brodie Granger (UBC), Douw Steyn (UBC), as well as Ellen Petticrew, Phil Owens, and Ken Otter (all UNBC). The research was funded in-part by the Environmental Damages Fund (Environment and Climate Change Canada), the Natural Sciences and Engineering Research Council of Canada, and the University of Northern British Columbia's Office of Research and Graduate Programs. Thanks to two anonymous referees for their constructive comments that led to an improved paper.

CONFLICT OF INTEREST

The authors declare that there is no conflict of interest regarding the publication of this article.

AUTHOR CONTRIBUTIONS

H.D.T. conducted the field project, conducted the analysis, and wrote the manuscript with direction and assistance from S.J.D. P.L.J. provided guidance throughout the meteorological analysis and with manuscript preparation. B.E.L. provided guidance regarding physical limnology content and with manuscript preparation.

ORCID

Hadleigh D. Thompson  <https://orcid.org/0000-0001-5145-5951>

REFERENCES

- Antenucci, J.P. and Imberger, J. (2003) The seasonal evolution of wind/internal wave resonance in Lake Kinneret. *Limnology and Oceanography*, 48(5), 2055–2061. <https://doi.org/10.4319/lo.2003.48.5.2055>.
- Bakri, T., Jackson, P.L. and Doherty, F. (2017) A synoptic climatology of strong along-channel winds on the coast of British Columbia, Canada. *International Journal of Climatology*, 37(5), 2398–2412. <https://doi.org/10.1002/joc.4853>.
- Beedle, M.J., Menounos, B. and Wheate, R. (2015) Glacier change in the Cariboo Mountains, British Columbia, Canada (1952–2005). *The Cryosphere*, 9(1), 65–80. <https://doi.org/10.5194/tc-9-65-2015>.
- Berrisford, P., Dee, D., Poli, P., Brugge, R., Fielding, K., Fuentes, M., Kallberg, P., Kobayashi, S., Uppala, S., and Simmons, A. (2009). *The ERA-interim archive version 2.0*. Technical report. <https://doi.org/10.1111/j.1365-2664.2007.01373.x>
- Breckling, J. (1989) In: Breckling, J. (Ed.) *The Analysis of Directional Time Series: Applications to Wind Speed and Direction*, Vol. 61. New York, NY: Springer New York. <https://doi.org/10.1007/978-1-4612-3688-7>.
- de Jong, M.P.C. and Battjes, J.A. (2004) Seiche characteristics of Rotterdam harbour. *Coastal Engineering*, 51(5–6), 373–386. <https://doi.org/10.1016/j.coastaleng.2004.04.002>.
- Dee, D.P., Uppala, S.M., Simmons, A.J., Berrisford, P., Poli, P., Kobayashi, S., Andrae, U., Balmaseda, M.A., Balsamo, G., Bauer, P., Bechtold, P., Beljaars, A.C., van de Berg, L., Bidlot, J., Bormann, N., Delsol, C., Dragani, R., Fuentes, M., Geer, A.J., Haimberger, L., Healy, S.B., Hersbach, H., Holm, E.V., Isaksen, L., Kallberg, P., Kohler, M., Matricardi, M., McNally, A.P., Monge-Sanz, B.M., Morcrette, J.J., Park, B.K., Peubey, C., de Rosnay, P., Tavolato, C., Thepaut, J.N. and Vitart, F. (2011) The ERA-interim reanalysis: configuration and performance of the data assimilation system. *Quarterly Journal of the Royal Meteorological Society*, 137(656), 553–597. <https://doi.org/10.1002/qj.828>.
- Delacre, M., Lakens, D. and Leys, C. (2017) Why psychologists should by default use Welch's t-test instead of Student's t-test. *International Review of Social Psychology*, 30(1), 92–101. <https://doi.org/10.5334/irsp.82>.
- Gardner, J.T., English, M.C. and Prowse, T.D. (2006) Wind-forced seiche events on Great Slave Lake: hydrologic implications for the Slave River Delta, NWT, Canada. *Hydrological Processes*, 20(19), 4051–4072. <https://doi.org/10.1002/hyp.6419>.

- Gibson, P.B., Perkins-Kirkpatrick, S.E., Uotila, P., Pepler, A.S. and Alexander, L.V. (2017) On the use of self-organizing maps for studying climate extremes. *Journal of Geophysical Research Atmospheres*, 122(7), 3891–3903. <https://doi.org/10.1002/2016JD026256>.
- Grotjahn, R., Black, R., Leung, R., Wehner, M.F., Barlow, M., Bosilovich, M., Gershunov, A., Gutowski, W.J., Jr., Gyakum, J.R., Katz, R.W., Lee, Y.-Y., Lim, Y.-K. and Prabhat. (2016) North American extreme temperature events and related large-scale meteorological patterns: a review of statistical methods, dynamics, modelling, and trends. *Climate Dynamics*, 46, 1151–1184. <https://doi.org/10.1007/s00382-015-2638-6>.
- Hatam, I., Petticrew, E.L., French, T.D., Owens, P.N., Laval, B. and Baldwin, S.A. (2019) The bacterial community of Quesnel Lake sediments impacted by a catastrophic mine tailings spill differ in composition from those at undisturbed locations—two years post-spill. *Scientific Reports*, 9(1), 2705. <https://doi.org/10.1038/s41598-019-38909-9>.
- Heaps, N.S. (1984) Vertical structure of current in homogeneous and stratified waters. In: Hutter, K. (Ed.) *Hydrodynamics of Lakes: CSIM Lectures*. New York: Springer Verlag Wein, pp. 153–207. https://doi.org/10.1007/978-3-7091-2634-9_5.
- Hernández-Henríquez, M.A., Sharma, A.R., Taylor, M., Thompson, H.D. and Déry, S.J. (2018) The Cariboo Alpine Mesonet: sub-hourly hydrometeorological observations of British Columbia's Cariboo Mountains and surrounding area since 2006. *Earth System Science Data*, 10(3), 1655–1672. <https://doi.org/10.5194/essd-10-1655-2018>.
- Hewitson, B.C. and Crane, R.G. (2002) Self-organizing maps: applications to synoptic climatology. *Climate Research*, 22, 13–26. <https://doi.org/10.3354/cr022013>.
- Hodges, B.R., Imberger, J., Laval, B.E. and Appt, J. (2000) Modeling the hydrodynamics of stratified lakes. In: *Hydroinformatics 2000 Conference*, Iowa Institute of Hydraulic Research, pp. 23–27.
- Imam, Y.E., Laval, B., Pieters, R. and Lawrence, G. (2013) The strongly damped baroclinic response to wind in a multibasin reservoir. *Limnology and Oceanography*, 58(4), 1243–1258. <https://doi.org/10.4319/lo.2013.58.4.1243>.
- Kohonen, T. (1982) Self-organized formation of topologically correct feature maps. *Biological Cybernetics*, 43, 59–69. <https://doi.org/10.1007/BF00337288>.
- Kohonen, T. (2003) The self-organizing map. *Proceedings of the IEEE*, 78(9), 1464–1480.
- Kohonen, T., Schroeder, R.M. and Huang, T.S. (2001) *Self-Organizing Maps*, 3rd edition. Berlin, Heidelberg: Springer-Verlag, p. 528.
- Laval, B.E., Imberger, J., Hodges, B.R. and Stocker, R. (2003) Modeling circulation in lakes: spatial and temporal variations. *Limnology and Oceanography*, 48(3), 983–994. <https://doi.org/10.4319/lo.2003.48.3.0983>.
- Laval, B.E., Morrison, J., Potts, D.J., Carmack, E.C., Vagle, S., James, C., McLaughlin, F.A. and Foreman, M. (2008) Wind-driven summertime upwelling in a fjord-type lake and its impact on downstream river conditions: Quesnel Lake and river, British Columbia, Canada. *Journal of Great Lakes Research*, 34(1), 189–203. [https://doi.org/10.3394/0380-1330\(2008\)34](https://doi.org/10.3394/0380-1330(2008)34).
- Laval, B.E., Vagle, S., Potts, D., Morrison, J., Sentlinger, G., James, C., McLaughlin, F. and Carmack, E.C. (2012) The joint effects of riverine, thermal, and wind forcing on a temperate fjord lake: Quesnel Lake, Canada. *Journal of Great Lakes Research*, 38(3), 540–549. <https://doi.org/10.1016/j.jglr.2012.06.007>.
- Loikith, P.C., Lintner, B.R. and Sweeny, A. (2017) Characterizing large-scale meteorological patterns and associated temperature and precipitation extremes over the northwestern United States using self-organizing maps. *Journal of Climate*, 30, 2829–2847. <https://doi.org/10.1175/JCLI-D-16-0670.1>.
- Marcos, M., Monserrat, S., Medina, R., Orfila, A. and Olabarrieta, M. (2009) External forcing of meteorological tsunamis at the coast of the Balearic Islands. *Physics and Chemistry of the Earth*, 34(17–18), 938–947. <https://doi.org/10.1016/j.pce.2009.10.001>.
- Petticrew, E.L., Albers, S.J., Baldwin, S.A., Carmack, E.C., Déry, S. J., Gantner, N., Graves, K.E., Laval, B., Morrison, J., Owens, P. N., Selbie, D.T. and Vagle, S. (2015) The impact of a catastrophic mine tailings impoundment spill into one of North America's largest fjord lakes: Quesnel Lake, British Columbia, Canada. *Geophysical Research Letters*, 42(9), 3347–3355. <https://doi.org/10.1002/2015GL063345>.
- Rabinovich, A.B. and Monserrat, S. (1998) Generation of meteorological tsunamis (large amplitude seiches) near the Balearic and Kuril Islands. *Natural Hazards*, 18(1), 27–55. <https://doi.org/10.1023/A:1008096627047>.
- Schuenemann, K.C. and Cassano, J.J. (2010) Changes in synoptic weather patterns and Greenland precipitation in the 20th and 21st centuries: 2. Analysis of 21st century atmospheric changes using self-organizing maps. *Journal of Geophysical Research Atmospheres*, 115(D5), D05108. <https://doi.org/10.1029/2009JD011706>.
- Sharma, A.R. and Déry, S.J. (2016) Elevational dependence of air temperature variability and trends in British Columbia's Cariboo Mountains, 1950–2010. *Atmosphere—Ocean*, 54(2), 153–170. <https://doi.org/10.1080/07055900.2016.1146571>.
- Sheridan, S.C. and Lee, C.C. (2011) The self-organizing map in synoptic climatological research. *Progress in Physical Geography*, 35(1), 109–119. <https://doi.org/10.1177/0309133310397582>.
- Singer, I.A. (1967) Steadiness of the wind. *Journal of Applied Meteorology*, 6(6), 1033–1038. [https://doi.org/10.1175/1520-0450\(1967\)006<1033:sotw>2.0.co;2](https://doi.org/10.1175/1520-0450(1967)006<1033:sotw>2.0.co;2).
- Skific, N. and Francis, J. (2018) Self-Organizing Maps: A Powerful Tool for the Atmospheric Sciences, Applications of Self-Organizing Maps. Magnus Johnsson, IntechOpen, <https://doi.org/10.5772/54299>. Available from: <https://www.intechopen.com/books/applications-of-self-organizing-maps/self-organizing-maps-a-powerful-tool-for-the-atmospheric-sciences>.
- Spigel, R.H. and Imberger, J. (1980) The classification of mixed-layer dynamics of lakes of small to medium size. *Journal of Physical Oceanography*, 10(7), 1104–1121.
- Stahl, K., Moore, R.D. and McKendry, I.G. (2006) The role of synoptic-scale circulation in the linkage between large-scale ocean-atmosphere indices and winter surface climate in British

- Columbia, Canada. *International Journal of Climatology*, 26(4), 541–560. <https://doi.org/10.1002/joc.1268>.
- Stevens, C.L. and Lawrence, G.A. (1997) Estimation of wind-forced internal seiche amplitudes in lakes and reservoirs, with data from British Columbia, Canada. *Aquatic Sciences*, 59(2), 115–134. <https://doi.org/10.1007/s000270050080>.
- Valerio, G., Cantelli, A., Monti, P. and Leuzzi, G. (2017) A modeling approach to identify the effective forcing exerted by wind on a prealpine lake surrounded by a complex topography. *Water Resources Research*, 53(5), 4036–4052. <https://doi.org/10.1002/2016WR020335>.
- Vettigli, G. (2019). MiniSom: minimalistic and NumPy based implementation of the Self Organizing Map, <https://github.com/JustGlowing/minisom>.
- Yarnal, B. (1993) *Synoptic Climatology in Environmental Analysis: A Primer*. London: Belhaven Press, p. 195.
- Yarnal, B., Comrie, A.C., Frakes, B. and Brown, D.P. (2001) Developments and prospects in synoptic climatology. *International*

Journal of Climatology, 21(15), 1923–1950. <https://doi.org/10.1002/joc.675>.

SUPPORTING INFORMATION

Additional supporting information may be found online in the Supporting Information section at the end of this article.

How to cite this article: Thompson HD, Déry SJ, Jackson PL, Laval BE. A synoptic climatology of potential seiche-inducing winds in a large intermontane lake: Quesnel Lake, British Columbia, Canada. *Int J Climatol*. 2020;1–14. <https://doi.org/10.1002/joc.6560>